Research Article Vol. 15, No. 2 / 1 Feb 2024 / Biomedical Optics Express 641
Biomedical Optics EXPRESS

Multispectral indices for real-time and non-invasive tissue ischemia monitoring using snapshot cameras

JENS DE WINNE,[1,2,†*] ANOEK STRUMANE,[1,†] DANILO BABIN,[1] SIRI LUTHMAN,[2] HIEP LUONG,[1] AND WILFRIED PHILIPS[1]

[1]*Department of Telecommunications and Information Processing (TELIN) - PI Research Group, Ghent University-imec, 9000 Ghent, Belgium*
[2]*Interuniversity Micro-Electronics Center (IMEC) vzw, 3000 Leuven, Belgium*
[†]The authors contributed equally to this work.
[*]*jens.dewinne@ugent.be*

Abstract: An adequate supply of oxygen-rich blood is vital to maintain cell homeostasis, cellular metabolism, and overall tissue health. While classical methods of measuring tissue ischemia are often invasive, localized and require skin contact or contrast agents, spectral imaging shows promise as a non-invasive, wide field, and contrast-free approach. We evaluate three novel reflectance-based spectral indices from the 460 - 840 *nm* spectral range. With the aim of enabling real time visualization of tissue ischemia, information is extracted from only 2-3 spectral bands. Video-rate spectral data was acquired from arm occlusion experiments in 27 healthy volunteers. The performance of the indices was evaluated against binary Support Vector Machine (SVM) classification of healthy versus ischemic skin tissue, two other indices from literature, and tissue oxygenation estimated using spectral unmixing. Robustness was tested by evaluating these under various lighting conditions and on both the dorsal and palmar sides of the hand. A novel index with real-time capabilities using reflectance information only from 547 *nm* and 556 *nm* achieves an average classification accuracy of 88.48, compared to 92.65 using an SVM trained on all available wavelengths. Furthermore, the index has a higher accuracy compared to reference methods and its time dynamics compare well against the expected clinical responses. This holds promise for robust real-time detection of tissue ischemia, possibly contributing to improved patient care and clinical outcomes.

1. Introduction

A supply of oxygen-rich blood to tissue is essential to maintain cellular homeostasis and metabolic processes, thereby ensuring healthy tissue. Efficient venous blood flow is vital to carry away metabolic waste products. Skin ischemia, characterized by restricted blood supply to (a part of) skin tissue disrupts these mechanisms and results in tissue hypoxia. Monitoring skin ischemic conditions, therefore, holds diagnostic significance and finds relevance in various medical contexts, including the diagnosis and assessment of peripheral arterial disease [1], the localization of cancers [2], and the monitoring of wound healing [3]. Furthermore, it offers valuable insights for surgeons, allowing direct assessment of tissue states during surgical procedures. Traditional methods like oximeters, blood gas analysis, diffuse reflectance spectroscopy, and angiography often necessitate invasive procedures, skin contact or the use of contrast agents, and typically yield localized measurements. In contrast, our study seeks to overcome these limitations by investigating hyperspectral imaging (HSI) as an optical, non-invasive, and contrast-free approach to evaluating ischemic conditions in skin tissue.

HSI has already been shown to be capable of detecting changes in blood perfusion and oxygenation, using commercially available systems, such as the TIVITA© (Diaspective Vision,

#506084 https://doi.org/10.1364/BOE.506084
Journal © 2024 Received 15 Sep 2023; revised 14 Nov 2023; accepted 14 Nov 2023; published 4 Jan 2024

Biomedical Optics EXPRESS

Germany). As far as the author is aware, most studies make use of spatial or spectral line scanning techniques [4]. These systems have high spatial or spectral resolution but have relatively lower temporal resolution, making real-time feedback on the tissue parameters challenging. The potential for real-time monitoring becomes apparent with the evolution of snapshot cameras, recording the spectrum of one pixel in one instance ("shot"). This results in acquisition speeds up to 50 Hz but comes at the cost of reduced spatial and spectral resolution. In this study, we hypothesize that spectral information from a limited spectral range, using only a few wavelengths, is sufficient for the detection of ischemia in skin tissue, limiting computational demand and possibly increasing diagnostic accuracy. This work aims to identify these information-rich spectral bands in the limited spectral range of snapshot cameras and to construct indices capable of monitoring skin tissue ischemia in real time. To extract and validate these indices, a feasibility study was performed by inducing arm occlusion with a pressure cuff. This experiment generated an immediate and potent effect on the skin's reflectance spectrum and serves to establish the indices. To investigate a sufficiently large spectral range, we employed a dual snapshot system having 2 cameras in one housing. The system spans a spectral range of 460-840 *nm*, including two snapshot cameras measuring in the 460-590 *nm* and 605-840 *nm* range respectively.

Current state-of-the-art HSI methods evaluating ischemic conditions of skin tissue clearly show its potential, with more recent studies employing snapshot cameras, but they are often based on methods such as machine learning [5] and deep learning [6,7]. Such techniques require a large amount of training data, which is difficult to obtain in clinical practice. Hence, the models are built on simulated data, e.g. using (multi-layered) Monte Carlo simulations on a digital skin model. These methods require adaptation from the simulated data domain to the camera-specific domain, a challenging transformation that is still under investigation in current research [8]. Others use numerical methods but are targeted at tissue oxygenation estimates [9–11]. A few studies have already investigated the construction of numeric indices to assess ischemic conditions of (skin) tissue based on a subset of wavelengths from reflectance spectra [12,13]. Hence, we will compare the performance of our proposed method with those found in the literature. The first comparable index originates from Akbari et al., who derived an ischemia index to detect intestinal ischemia during surgery. The study was carried out in one pig and intestinal ischemia was simulated by clamping vessels that supplied an intestinal segment. Here, the performance of their different indices was also screened using SVMs. Holmer et al. designed different indices which are integrated into the TIVITA© system, which has been widely validated in different types of clinical studies, such as [14] and [15]. The indices were constructed with the aim of noninvasive evaluation of wound perfusion. In this case, validation was done by performing an arm occlusion study on the palmar side of the hands. Their *Tissue Hemoglobin Index* falls within the spectral range of this study and will be used for comparison. Additionally, our proposed ischemia indices will be compared with estimated tissue oxygenation values using a modified version of the Beer-Lambert law (BLL) [16]. The BLL is a widely applied linear estimation method of the concentration of chromophores in media based on light absorption patterns. Here, we consider haemoglobin to be a notable absorber, as it is the most dominant in the investigated spectral range.

Three novel ischemia indices are proposed solely based on the reflectance intensities of light in 2 or 3 wavelengths. Their diagnostic ability to detect ischemic conditions in skin tissue is tested on hyperspectral images of healthy and ischemic dorsal and palmar hands, obtained by performing an upper arm occlusion study. Two experiments are performed: an initial experiment encompassing 15 subjects and using ideal lighting conditions to construct the ischemia indices, and a follow-up experiment on 12 subjects to validate the robustness of the developed indices to different experimental conditions, using a simple desk light as the light source, allowing stray light and limiting the dynamic range of the data using a white background. A complete image processing pipeline is developed. The ability of the proposed indices to assess skin ischemia is

Biomedical Optics EXPRESS

compared to the reference methods from the literature, by evaluating their classification accuracy of healthy versus ischemic skin tissue using binary SVMs. The proposed method is also compared to the baseline classification method by training SVMs directly on the reflectance information.

2. Materials and methods

2.1. Upper arm occlusion protocol

Upper-arm occlusion studies were performed on human volunteers. In total, 27 healthy subjects participated in the study with none of the participants reporting previous conditions, skin- or cardiovascular disease. The initial study comprised 15 subjects (8 Caucasian males, 4 Asian males, and 3 Caucasian females), and the follow-up study comprised 12 subjects (6 Caucasian males, 3 Asian males, and 3 Caucasian females). Skin types ranged from I-III on the Fitzpatrick scale [17]. The approval of the ethics committee was given by the Ethics Committee of the University Hospital of Ghent (B6702023000034) and the informed consent of all participants. The protocol of the occlusion study is based on [5].

To obtain hyperspectral images of healthy and ischemic skin tissue, a pressure cuff was applied to the left upper arm to occlude the lower arm. To ensure both arterial and venous occlusion, an inflation pressure of 200 mmHg was maintained. Measurements of the arm were taken in a seated position. Three images were taken from the hand of each test subject. One before the cuff was applied, one 5 minutes after the cuff was applied with the inflation pressure maintained, and one directly after its release. To ensure the lower arms were kept at the same location throughout the measurements, markings were applied to the background. For one subject, a recording was made during the occlusion period at a frame rate of 5 Hz to study the dynamic responses on the proposed ischemia indices. This frame rate was chosen to minimize the amount of data stored.

2.2. Data acquisition

2.2.1. Hyperspectral imaging system

Reflectance spectra were acquired using IMEC's snapshot VIS+NIR camera. The HSI camera combines two snapshot mosaic cameras, namely the *xiSpec MQ022HG-IM-SM4X4-VIS* with a spectral range of 460 - 590 nm over 16 wavelengths, and the *xiSpec MQ022HG-IM-SM4X4-RN* with a spectral range of 605 - 840 nm over 15 wavelengths (XIMEA, Germany) in one housing. Both cameras have a spatial resolution of 1088 by 2048 pixels and a pixel pitch of 5.5 µm. FWHM values range between 6 and 18 nm. Both were equipped with lenses with a focal length of 25 mm (C-series VIS-NIR lens, Edmund Optics, Inc., USA). Throughout this paper, we will refer to the first as the 'VIS' camera and the latter as the 'NIR' camera.

The HSI camera was mounted on a customized stage, directly above the hand, to ensure the camera sensor was as parallel to the skin tissue as possible. The system was mounted at a working distance of 50 cm, with the different light sources placed at an oblique angle with respect to the hand to minimize specular reflections. RAW data and metadata of the VIS and NIR cameras were collected and stored directly in local storage. An overview of the setup is shown in Fig. 1.

2.2.2. Experiments

In the initial experiment, the experimental conditions were idealized and extracted data was used to construct the ischemia indices. To illuminate the scene, 2 LED bars having balanced and temporally stable lighting (EFFI-FLEX-HSI-300-KIT-ELS-350-24V, Effilux, France) are mounted above the hand. The images were taken from the dorsal side of the hand. To reduce stray light, all ambient light sources were turned off to reduce signal noise. The spectrum of the LED light source is shown in Fig. 1(c). It has sufficient power and a rather flat profile in the range of 470 to 800 nm, which makes it a suitable light source given the spectral range of the HSI system. In addition, a background with low reflectivity across the spectral range of the camera

Biomedical Optics EXPRESS

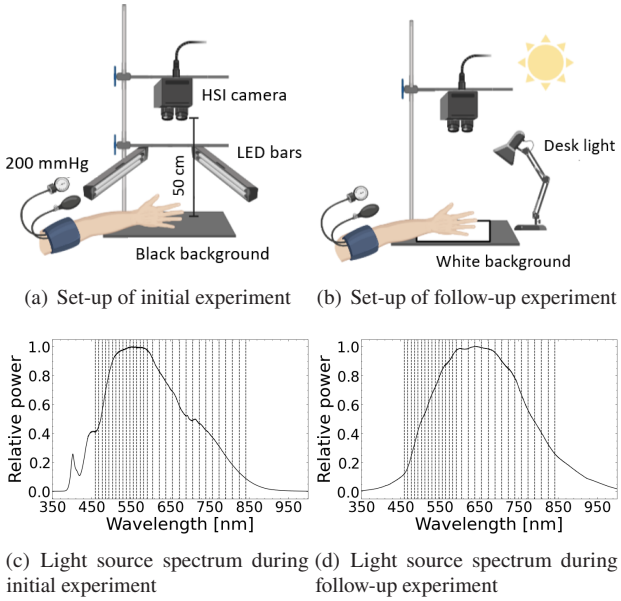

(a) Set-up of initial experiment (b) Set-up of follow-up experiment

(c) Light source spectrum during initial experiment (d) Light source spectrum during follow-up experiment

Fig. 1. A set-up with idealized acquisition conditions (a), with minimal stray light and uniform illumination (c) was used to develop the ischemia indices. To evaluate robustness of the indices, their performance was evaluated on data acquired in non-idealized conditions (b), in the presence of ambient light and under non-uniform illumination (d). Vertical black lines indicate the central wavelengths of the HSI camera.

was used to optimize the dynamic range of the images. This experiment encompasses data from 15 subjects and experimental conditions are considered ideal.

To show the robustness of the proposed ischemia indices monitoring skin ischemia in a different experimental scenario, a follow-up experiment is performed for 12 subjects. Here, images were taken from both the dorsal and palmar sides of the hand. In this experiment, one simple halogen desk light is used and stray light (outdoor sunlight) is allowed. In addition, a reflective background is used to enforce a limited dynamic range of the skin and amplify stray light. This data is used to evaluate the constructed indices and models throughout this work under nonideal conditions.

2.3. Image pre-processing

2.3.1. Radiometric calibration

Pre-processing is performed to convert raw sensor data into reflectance data. The same pre-processing is applied for every wavelength of both the VIS and NIR hypercubes. First, raw images are dark corrected and demosaicked. To compensate for spectral imperfections inherent to the use of the Fabry-Pérot interference filter arrays on the image sensor, images are further convolved with a radiometric correction matrix supplied by the manufacturer (Imec, Belgium). More details can be found in [18]. Afterwards, an angularity correction step is applied to correct chromatic lens aberration in the spectral domain. Finally, images are white balanced by dividing by an image of a uniform diffuse white reference tile covering the full field-of-view (Spectralon 95%, SphereOptics GmbH), taking into account the different integration times of the images and the white reference tile. Finally, an additional spectral correction is done for every wavelength based on color checker chart measurements (ColorChecker Classic Mini, Calibrite) from the HSI camera and a reference spectrometer (HR4000, Ocean Optics). This is done only once for the initial experiment. This additional processing step is essential to ensure that the spectra of the VIS

Biomedical Optics EXPRESS

and NIR cameras can be combined for further analysis. Further details on this implementation and the white balancing can be found in the provided Supplement 1.

2.3.2. Segmentation, registration, and superpixel computation

The complete processing pipeline is visualized in Fig. 2. After radiometric calibration, the images of both cameras were cropped to align their field of view. Next, images of the NIR camera were registered to those of the VIS camera using an automatic translational registration algorithm, using the SimpleElastix medical registration library (2.2.1) in Python (3.10.4). After registration, they were merged to construct a full hypercube. Segmentation of the hand was performed by thresholding the image at 774 nm, which empirically resulted in an optimal segmentation mask. Thresholding was based on the triangle algorithm implementation of scikit-image (0.19.3) and was applied to every wavelength of the hypercube. Finally, superpixels were computed from the hypercube. This was done to increase the sample size of the data for training and testing the classifiers compared to training and testing on the images as a whole. As a limited number of 27 subjects are included in the study, the analysis was performed superpixel-wise. It is preferred to pixel-wise comparison, as the registration between both cameras is not perfect. Also, it groups pixels with similar spectra spatially, which considers ischemic conditions of small and spectrally similar tissue regions as homogeneous, making more sense from a physiological point of view whilst also less prone to noise. For the computation of the superpixels, the implementation of the SLIC algorithm in scikit-image (0.19.3) was used. This performs k-means clustering over the spectral dimension and is performed separately for every hypercube, resulting in different superpixels for every hypercube. This helps to cope with inter-subject variations. The number of segments was chosen to be 150 and the compactness 0.1. These same parameters were used for every hypercube, clearly visualizing the computed ischemia indices and resulting in a sufficient amount of training samples for the classifiers. The ischemia indices were then calculated for each superpixel, and the reflectance spectra of a single superpixel were calculated as the mean spectra of all pixels belonging to that specific superpixel.

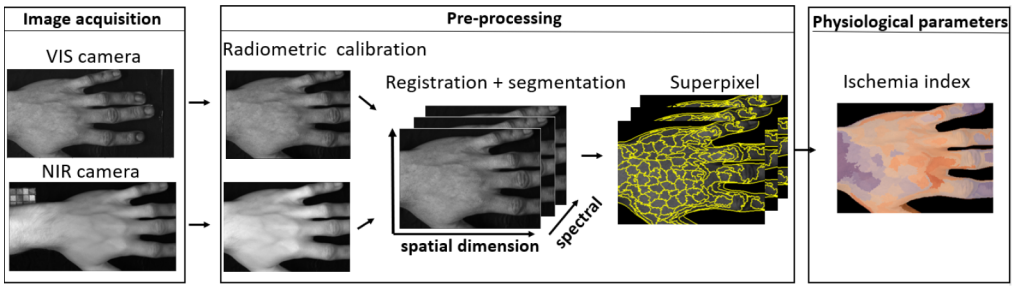

Fig. 2. The raw demosaicked images from the camera were spectrally corrected and white balanced. Next, images of the VIS and NIR camera were registered to form the full hypercube and the hand was segmented from the background. To generate a sufficient amount of training samples for classification, superpixels were. Finally, the ischemia indices, oxygenation values and mean reflectance spectra were computed per superpixel, resulting in a 2D map.

2.4. Tissue ischemia indices and oxygenation

Indices were constructed based on wavelength differences and ratios of reflectance values from the two cameras. Three indices were extracted: one with data from the VIS camera (I_{vis}), one with data from the NIR camera (I_{nir}), and one index using data from both the VIS and the NIR camera (I_{vnir}). The number of wavelengths was deliberately kept small to ensure robustness and real-time processing.

Biomedical Optics EXPRESS

To construct I_{vis}, all unique 2-wavelength combinations from the 16 possible wavelengths were evaluated, resulting in a total of 120 candidates. The differentiation between healthy (before cuff) and ischemic (during cuff) superpixels was maximized. For every possible index, its values were calculated for all healthy and ischemic superpixels of all subjects, and two separate datasets were made. The non-parametric Mann-Whitney U test was performed for every unique combination and the one with the most significant difference between healthy and ischemic (lowest p-value) was selected as I_{vis}. The same procedure was done for I_{nir} and I_{vnir}. This resulted in the below optimal ischemia indices, where R_x depicts the reflectance value at wavelength x in nm and the index was constructed in such a way that its value will be higher in ischemic conditions. Average reflectance and absorbance spectra are shown in the Supplement 1.

$$I_{vis} = R_{556} - R_{547} \tag{1}$$

$$I_{nir} = \frac{R_{740}}{R_{808}} \tag{2}$$

$$I_{vnir} = \frac{R_{495} - R_{605}}{R_{740}} \tag{3}$$

The performance of the proposed novel indices was compared to two indices originating from the literature. It must be noted that the wavelengths available in this work do not exactly match those from the literature. In these cases, either the nearest wavelength (if the mismatch was smaller than 3 nm) or a quadratic interpolation of the two nearest wavelengths available in the hypercube was used (the maximal mismatch was 8 nm). A table with reference ischemia indices and more information is given in Table 1. Note that these indices were developed using different acquisition systems and different data sets. The first ($I_{ref,1}$) originates from [12]. Here, C is a constant coefficient to normalize their index. For the purpose of this work, it is not necessary to determine and apply the normalization coefficient, as this would not affect the performance of the SVM. The first derivative of the reflectance value R at wavelength x nm is noted as R'_x. The second ($I_{ref,2}$) originates from [13]. The s values also represent normalization constants and A represent absorbance values. Following the same reasoning as for the previous index, the constant s was omitted. Absorbance values are estimated by negating the logarithm of the reflectance value. In addition, performance was compared to tissue oxygenation estimates derived from a modified version of the Beer-Lambert law [16]. More details on the implementation of the oxygenation algorithm are found in the Supplement 1.

Table 1. The ischemia indices from literature.

Ischemia index	# wavelengths	HSI system	Spectral range and resolution	Application	Reference
$I_{ref,1} = \lvert\sum_{757}^{824} R'_i\rvert + \sum_{757}^{824} R'_i$	6	2 line-scan cameras	400-1700 nm (5 nm)	Intestinal ischemia	([12])
$I_{ref,2} = \frac{\text{mean}(A_{785:825})}{\text{mean}(A_{530:590})}$	10	push-broom spectrograph	500-1000 nm (1 nm)	Wound perfusion	([13])

2.5. Binary classification with support vector machines

After completing the pre-processing pipeline in 2.3, the performance of the indices for ischemia diagnosis was evaluated by using them as training data for a Support Vector Machine (SVM), which is a frequently used classifier in the domain of medical image analysis. The performance of an SVM was found to be superior compared to a random forest classifier for the given application. Hence, SVMs are used as state-of-the-art reference method throughout this study. More details on this comparison are provided in the Supplement 1. As the focus of this study lies on the detection and monitoring of ischemia, superpixel images before and during the occlusion are

Biomedical Optics EXPRESS

labelled as *healthy* and *ischemic* samples respectively, and these are used for training the SVM. Images after the release of the cuff are expected to differ significantly from those before, as reactive hyperemia occurs and are thus not used for training [19]. After training the models, they were tested in the follow-up experiment to show robustness in non-idealized experimental conditions. An overview is given in Fig. 3.

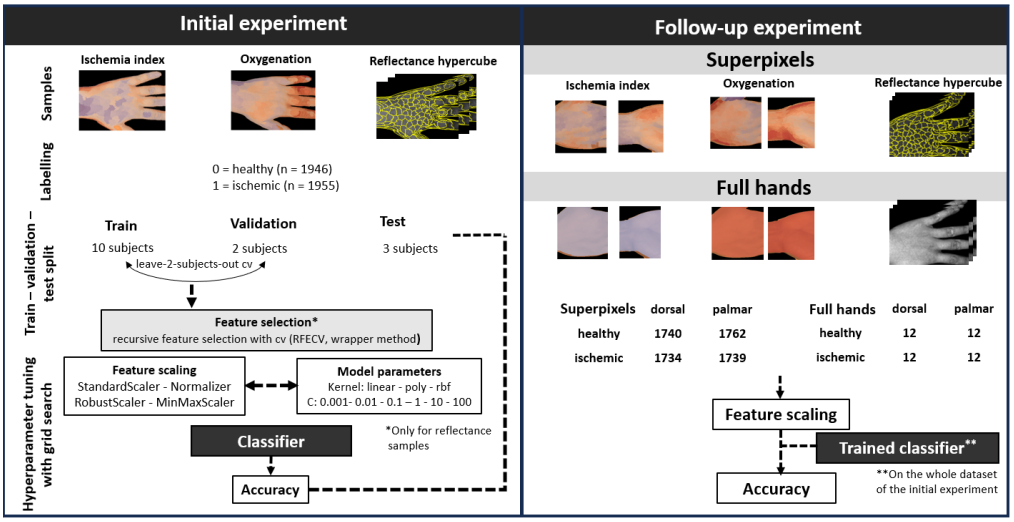

Fig. 3. Classifiers using the ischemia indices, oxygenation values and mean reflectance of superpixels are trained and tested during the initial experiment. Afterwards, the models are tested for robustness on the data of the follow-up experiment, which additionally contains data from both dorsal and palmar sides of the hand and experimental conditions are considered non-ideal.

Training and testing SVMs on data of the initial experiment The dataset is considered balanced with 1934 healthy samples and 1915 ischemic samples. When training on ischemia indices, the index of a superpixel was considered a sample. In this case, the SVM will act solely as a model that selects the optimal threshold value to classify between healthy and ischemic samples. In the case of training with reflectance values, the mean reflectance spectra of the superpixel were considered as a sample. The samples were split into a train and test set. The test set consisted of 3 randomly selected subjects that are completely left out of training. The training and validation set (12 subjects) was used to tune the hyperparameters using the grid search algorithm with the accuracy score as a performance metric. Cross-validation was performed by leave-2-subjects-out cross-validation, meaning that at each cross-validation the model is trained on 10 subjects and validated on 2 subjects. This was done for every possible combination (66 splits) to ensure the trained model performs well for every subject and subject-specific bias is reduced. The obtained accuracy using this cross-validation method is referred to as the validation accuracy.

The first step in the training procedure is model hyperparameter tuning. For this, the feature scaling method, kernel, and regularization parameter C were considered hyperparameters. The ranges for these hyperparameters are shown in Fig. 3. For the reflectance data-based models, feature selection was performed first with the standard hyperparameters of the SVM (*StandardScaler*, linear kernel, and C of 1). This was done using recursive feature elimination, which is a wrapper method. This corresponds with the selection of an optimal subset of wavelengths that leads to the highest accuracy score with the mentioned cross-validation method. Then, for each subset model, the same hyperparameters were optimized. As for models trained

Biomedical Optics EXPRESS

on ischemia indices, they only have one feature: the index value. Hence, no additional feature selection was performed. Next, the model with optimal hyperparameters was trained in the 12 subjects of the training set and the performance was evaluated in the test set of 3 subjects.

Evaluating the robustness of trained SVMs on the follow-up experiment Performance is evaluated in two ways: superpixel-wise, i.e. classification of a single superpixel, and on the dorsal and palmar side of the hand as a whole. For the latter, the mean spectra of every superpixel were again averaged and considered as one sample for classification. Ischemic indices were calculated from these averaged spectra. In total, the number of samples in each case is shown in Fig. 3.

3. Results

3.1. Initial experiment

Hyperparameter tuning The optimal hyperparameters were determined for each SVM, and are shown in Table 2 for ischemia index and oxygenation-based SVMs. All models have the highest accuracy using *StandardScaler*, while the kernel type and regularization parameter C vary. However, obtained accuracy scores did not vary much by kernel type or C, as the SVM only has a single feature: the index or oxygenation value. Table 3 shows the optimal hyperparameters for reflectance-data-based SVMs. Four reflectance-data based SVMs were trained: one trained on 2 wavelengths (same amount as I_{vis} and I_{nir}), one on 3 wavelengths (same amount as I_{vnir}), one on 12 wavelengths (optimal accuracy using recursive feature selection) and one on the full wavelength set. Optimal hyperparameters and wavelength subsets are shown in Table 3, where SVM_x indicates an SVM trained on x amount of wavelengths. Again, a *StandardScaler* is found to be optimal in every case. Compared to ischemia index and oxygenation-based SVMs, the performance of the models is more sensitive to the chosen kernel and C value.

Table 2. The optimal hyperparameters of the index and oxygenation-based SVMs determined.

Hyperparameter	I_{vis}	I_{nir}	I_{vnir}	$I_{ref,1}$	$I_{ref,2}$	$SatO_2$
Feature scaling	StandardScaler	RobustScaler	RobustScaler	StandardScaler	StandardScaler	StandardScaler
Kernel	rbf	linear	linear	rbf	rbf	linear
C	1	0.1	0.1	0.1	1	0.1

Table 3. The optimal hyperparameters of reflectance data-based SVMs.

Hyperparameter	SVM_2	$\boldsymbol{SVM_3}$	SVM_{12}	$\boldsymbol{SVM_{all}}$
Feature scaling	StandardScaler	StandardScaler	StandardScaler	StandardScaler
Kernel	rbf	linear	linear	linear
C	100	100	100	10
Selected wavelengths (nm)	529, 590	529, 590, 689	467, 503, 511, 520, 529, 538, 547, 555, 573, 590, 689, 774	all

Classification accuracy The performance during validation and testing in terms of superpixel accuracy is provided in the overview Table 4. The SVM based on I_{vnir} has the highest test accuracy compared to all other index and oxygenation-based SVMs, with a value of 78.36. Remarkably, I_{vnir} has a higher test accuracy compared to SVM_3 and I_{nir} performs better than SVM_2. Moreover, I_{nir} and I_{vnir} achieve higher accuracy compared to the references from literature. Here, it should be noted that the computation for $I_{ref,1}$ often results in 0. However, at the cost of increasing the size of the wavelength subset, the highest overall test accuracy is achieved by training an SVM on all wavelengths (89.88).

Biomedical Optics EXPRESS

Table 4. Overview of the accuracy scores of all SVMs in the data of the initial experiment (15 subjects) and follow-up experiment (12 subjects). Provided values from the initial experiment are averages over all cross-validations during validation, along with the standard deviation. In addition, accuracy scores on the test set of 3 subjects is also given.

		Initial experiment		Follow-up experiment			
SVM	Wavelengths	Validation accuracy	Test accuracy	Superpixel accuracy		Full hands accuracy	
				Dorsal	Palmar	Dorsal	Palmar
I_{vis}	2	68.89 +- 6.12	64.92	85.29	91.66	100	100
I_{nir}	2	65.67 +- 6.52	71.96	74.61	87.52	75.00	100
I_{vnir}	3	78.23 +- 5.68	78.36	78.61	75.29	100	83.33
$I_{ref,1}$	6	61.85 +- 4.98	65.17	71.62	80.38	79.17	87.50
$I_{ref,2}$	10	51.10 +- 1.30	52.62	50.34	49.53	45.83	41.67
$SatO_2$	31	67.59 +- 8.07	65.30	74.50	74.75	83.33	87.50
SVM_2	2	72.12 +- 6.60	69.89	84.28	80.78	95.83	75.00
SVM_3	3	72.90 +- 7.26	68.89	84.28	86.09	91.67	87.50
SVM_{12}	12	96.29 +- 3.04	85.15	93.96	93.09	91.67	95.83
SVM_{all}	31	95.85 +- 3.22	89.88	94.07	91.23	91.67	91.67

I_{nir} and I_{vnir} outperform oxygenation-based SVMs based on all 31 available wavelengths. Statistical analysis using the non-parametric Mann-Whitney U-test shows that dorsal Sat_O2 values are significantly different between the initial and follow-up experiment, both before (84.89 +- 9.38 versus 76.06 +- 6.72) and during (76.96 +- 8.93 versus 63.47 +- 8.01) the occlusion using a significance level of 0.05, showing high inter-experiment and inter-subject variability. To illustrate inter-subject variability, a Kruskal-Wallis test followed by Dunn's test was performed for dorsal $SatO_2$ values before occlusion in the initial experiment. All 105 unique pairwise comparisons were made between the 15 subjects, and 84 were found to be significant ($p < 0.05$), meaning 80% of pairwise combinations have a significantly different baseline $SatO_2$ value.

Color-coded maps Figure 4(a) shows color-coded maps of ischemia indices and tissue oxygenation values before, during, and after upper arm occlusion for a subject overlayed on a false RGB reconstruction, providing spatial information on the distribution of these values on the hand. In all cases, skin ischemia can be visually detected by an evident decrease in the value of these parameters. After occlusion, the levels increase again.

3.2. Follow-up experiment

Classification accuracy Table 4 provides an overview of the accuracy scores of all trained models on the data from the follow-up experiment. The 2-wavelength index I_{vis} outperforms all other ischemia index and oxygenation-based SVMs, having high accuracy scores on superpixel data on both the dorsal (85.29) and palmar (91.66) side of hands and a perfect classification for full hand data. Only SVM_{12} and SVM_{all} have better superpixel performance, at the cost of using a larger subset of wavelengths. However, their accuracy in full-hand data is slightly worse, with SVM_{12} having one misclassification and SVM_{all} having two misclassifications out of 24 samples. In addition, I_{vis} performs better than SVM_2, indicating that this numeric ischemia index method is more robust in this experiment. Again, the proposed indices show higher accuracy compared to references from the literature, but I_{nir} has a comparable performance compared to $I_{ref,1}$ on superpixels. Remarkably, all models have been trained on superpixels of the dorsal side of the hand, but their performance is comparable to or even slightly better on palmar superpixels during the follow-up experiment.

Biomedical Optics EXPRESS

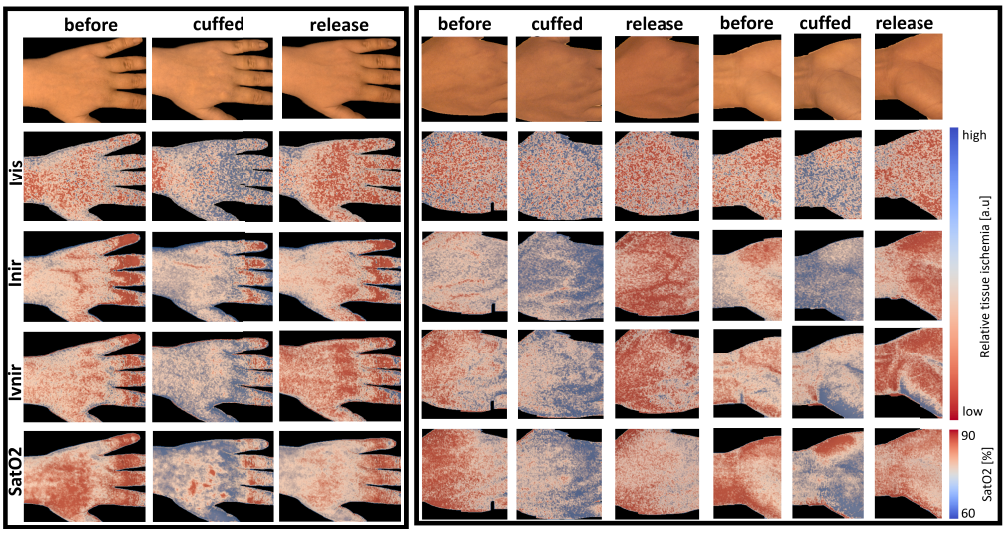

(a) Initial experiment (b) Follow-up experiment

Fig. 4. From top to bottom: images of false RGB reconstruction, *Ivis*, *Inir*, *Ivnir* and $SatO_2$ before, during, and after occlusion for subject 5. A decrease in the values is evident during occlusion as the images turn blue, indicating a low value. After occlusion, the hands become red again. The color bar is the same for all 3 images of a certain physiological parameter. The *coolwarm* colorbar from the matplotlib library was chosen for visualization. Values are displayed such that they have a low value during occlusion.

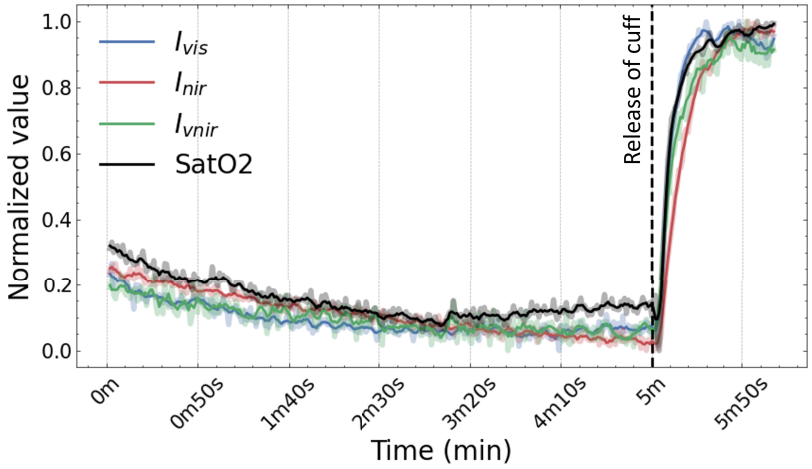

Fig. 5. For one subject, a video recording was made and the median index and oxygenation value over the hand is plotted during the occlusion. The pressure cuff was inflated at $0m$ and was kept inflated for 5 minutes, after which the pressure was released. The dynamic response of the ischemia indices and oxygenation values is clearly shown. Lines correspond with the filtered signals, and the envelope corresponds with the raw signal.

Color-coded maps Figure 4(b) and Fig. 4(c) show color-coded superpixel images of the proposed ischemia indices and the oxygenation values for one subject during the follow-up experiment for both the dorsal and palmar sides of the hands. Similar to Fig. 4(a), skin tissue

Biomedical Optics EXPRESS

ischemia can be visually detected by an evident decrease in all index and oxygenation values during occlusion. After occlusion, levels increase again. During the follow-up experiment, images had to be cropped to the centre of the hand due to experimental restrictions.

3.3. Dynamic response of the ischemia indices during occlusion

The time responses of the proposed ischemia indices and the oxygenation values during a recording in a subject are shown in Fig. 5. The video recording was resampled from 5 to 1 Hz. 0 seconds indicates the start of the occlusion. The time plot was filtered with a moving average of 5 frames. For ease of comparison, time responses are normalized between 0 and 1. During occlusion, the values of the ischemia indices start to decrease and appear to stabilize after approximately 3 minutes. When the pressure cuff is released, a steep increase is observed, stabilizing after 50 seconds. At the moment of release, reactive hyperemia was visually observed at the hands of the subjects as they became redder. The body responds to release with a highly increased arterial inflow of blood to the arm, drastically increasing the total amount of blood and blood oxygenation [19]. This dynamic response can be captured by real-time mapping of the proposed ischemia indices.

4. Discussion

Through SVM classification, our results emphasize the efficacy of the proposed indices. I_{vnir}, based on information at 495 *nm*, 605 *nm*, and 740 *nm* exhibits superior diagnostic accuracy in an initial experiment, compared to oxygenation-based SVMs, reference indices from the literature, and reflectance data-based SVMs using three wavelengths. This index reveals the efficiency of a targeted approach. Further validation in non-ideal experimental conditions and on different hand surfaces demonstrates the robustness of the proposed indices. Remarkably, an ischemia index based on 547 *nm* and 556 *nm* achieves the highest accuracy on both the dorsal and palmar sides of the hand, emphasizing the indices' capacity to accurately identify ischemic tissue regions under various lighting conditions and dealing with inter-subject variability. Models based on $SatO_2$ show less robustness, as these values are more prone to these variations. Models SVM_{12} and SVM_{all} have higher accuracy, but also use a larger subset of wavelengths, and are thus less suited for real-time visualization. The proposed approach has the potential to identify ischemia in multiple tissue types. However, the generalisability of the indices to other body regions and tissue types requires further research. In addition, the performance of the indices in a real clinical setting has yet to be evaluated and the assessment of their sensitivity is currently the subject of further work.

During this experiment, SVM_{12} has a slightly better performance than SVM_{all}. This finding is in line with other similar studies suggesting that the selection of a subset of wavelengths can improve diagnostic performance. For example, [20] found that 10 wavelengths closely reproduce results from 101 wavelengths in the 500-700 *nm* spectral range in their random forest-based tissue oxygenation model. Similarly, [21] studied the selection of wavelengths for the estimation of skin tissue oxygenation using a similar Beer-Lambert model in the spectral region 450 - 850 *nm* and found subsets between 516 and 580 *nm* providing more accurate estimations. By selecting a specific subset, redundant information is reduced by leaving out noisy data and wavelengths that do not contain much information on the ischemic conditions of skin tissue.

Figure 6 shows the wavelengths employed in the proposed ischemia indices compared to those selected by the reflectance-data-based SVMs (using recursive feature selection), overlaid with the absorption spectrum of blood. In general, $500 - 600$ *nm* is identified as a key spectral region, being selected by recursive feature elimination and the region for I_{vis}, which originates from the VIS camera. This is in line with the findings from the literature discussed in the previous paragraph ([20], [21]). As opposed to tissue ischemia, these studies focus on tissue oxygenation. In this spectral region, the absorption of blood is high, leading to a more dominant absorption

Biomedical Optics EXPRESS

of blood compared to that of other chromophores present in skin tissue. In addition, the region contains the double absorption peak of oxygenated blood and spans a few isosbestic points. The isosbestic points could allow the models and indices to normalize values for the hematocrit value of the blood, as absorption of oxy- and deoxygenated blood are equal and these points indicate the amount of blood. The wavelengths selected in SVM_2 are 529 *nm* and 590 *nm*, being an isosbestic point and a wavelength where the difference in absorption between oxy- and deoxygenated blood is high. The same is concluded for the wavelengths of I_{vis}, where 547 *nm* is close to the isosbestic point and 556 *nm* has a relatively high difference.

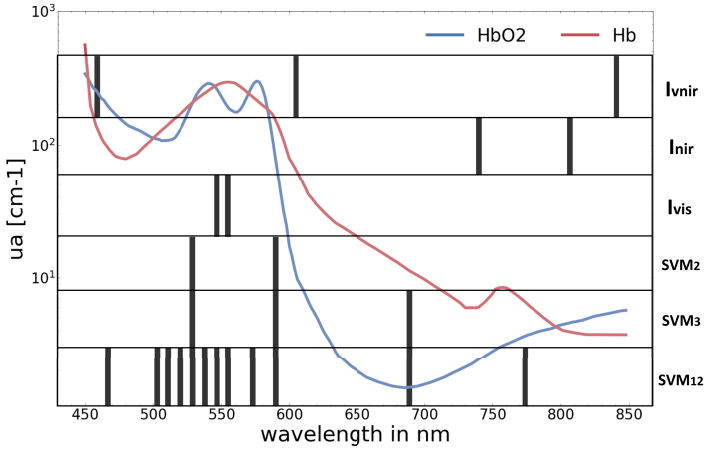

Fig. 6. Overlay of the selected wavelengths of the reflectance data-based SVMs (by recursive feature elimination), and proposed ischemia indices on the absorption spectra of blood. All best-performing models seem to use at least 1 isosbestic point and 1 point where the absorption between HbO_2 and *Hb* is highly different. Most wavelengths of the models are also located in the 500 - 600 *nm* spectral region. The values of oxy and deoxyhaemoglobin are taken from *https://omlc.org/spectra/hemoglobin*.

When mapping the indices to the hand in color-coded images (Fig. 4), they show a clear decrease during occlusion and an increase during the release of the cuff. However, there are spatial differences in these values on the same image of the hand. These are evident on the wrist (a,c) and fingers (a). In addition, images of I_{nir} seem to capture information from underlying vessels, as they show spatial differences in vessel-like structures compared to the rest of the hand. Here, it should be noted that I_{vis} solely uses information from the VIS camera, while I_{nir} and I_{vnir} use information from the NIR camera. As longer wavelengths penetrate the skin deeper ([22], [23]), these indices derive information from slightly deeper tissue, while I_{vis} derives information from more superficial skin tissue. Future studies should investigate whether these spatial differences are due to the skin microvasculature or due to the experimental design of the study. Literature suggests that, for example, the microvasculature is different in fingers, which could lead to a difference in ischemic conditions detected by one index and not by another [24].

The time dynamics of the indices during the occlusion, as depicted in Fig. 5, are in line with the well-documented clinical time response of an arterial occlusion test: gradually decreasing during occlusion with a high peak and overshoot during release of the cuff. [19]. Reactive hyperemia was visually observed during measurements as the hands of the subjects became redder. The body responds to the ischemia-induced period by vasodilation, reducing resistance in the microvasculature and allowing a surge of blood flow to restore tissue deprived of oxygen. Quantitative characteristics of the oxygenation response curve, such as the deoxygenation slope, time-to-peak, and reoxygenation slope are shown to detect microvascular dysfunction and to

Biomedical Optics EXPRESS

assess the general vascular health status of a patient [19]. Abelmalak et al. [25] correlate preoperative values with serious postoperative complications. The novel ischemia indices thus hold promise in assessing similar physiological conditions in real time. However, recordings should be made during longer time periods, both before and during the occlusion, to analyze the time dynamics of the complete occlusion and reperfusion response. As actual real-time visualization of the ischemia index maps was not the focus of this study, the operations involved in the image pre-processing are not yet optimized in terms of computational speed. However, to highlight the real-time capabilities of the proposed method, generating such an image using I_{vis} and I_{nir} from a radiometrically calibrated image takes a mere 38.59 µs, where the computation of $SatO_2$ maps using the Beer-Lambert law model takes 2.01 s. Values are averages over 10000 repetitions using an Intel Core i7 CPU.

The proposed ischemia indices can diagnose and monitor well in skin tones ranging from I-III on the Fitzpatrick scale but the performance could be impacted in darker skin. This has a higher melanin content absorbing more of the incident light. It is expected that the signal related to hemoglobin absorption would be reduced causing spectral features related to the absorption of hemoglobin to be less apparent in this case, leading to a possible drop in performance. It was investigated whether there were significant differences in superpixel-wise classification accuracy between Asian and Caucasian study participants in the follow-up experiment. This was done for all proposed ischemia indices and reference methods from Table 4. The details of this statistical analysis are provided in the Supplement 1. In case of SVM_3, SVM_{12} and SVM_{all} the accuracy is significantly lower for Asian participants ($\alpha = 0.05$). No significant difference was found for the proposed ischemia indices. This suggests that the indices may be more robust to skin tone, while the reflectance-based SVMs overfit towards Caucasian skin tone, which is predominant in the training set. However, care should be taken towards the interpretation of these results, as the amount of Asian participants ($n = 3$) was lower compared to Caucasian participants ($n = 9$). Future studies are encouraged to include a more diverse study group.

This study is prone to several limitations. In search of comparable numeric indices from the literature using HSI systems in the studied spectral range, $I_{ref,1}$ and $I_{ref,2}$ were found to be the most suitable. Although the proposed ischemia indices perform better compared to the reference indices from the literature, care must be taken to interpret these results. The reference indices were constructed using different experimental set-ups, including different HSI acquisition systems and applications. HSI systems from [12] and [13] have a much higher spectral resolution, which leads to the inclusion of a higher number of wavelengths in their indices. Furthermore, $I_{ref,1}$ was applied to intestinal tissue as opposed to skin tissue in this study. The computation of this index generated a lot of 0 values. This happens when the summation in the index as described in Table 1 has a negative outcome, as the sum of a negative value and its absolute value adds to 0. The original developers of this index did not have this problem in their study [12], indicating that this can be due to the different experimental set-up, HSI acquisition system, or targeted tissue. Additionally, no gold standard reference measurements, such as oxygenation measurements using the EPOS probe as in [6] were taken during the occlusion experiments. Following the described protocol of the study, the hands were assumed to be successfully occluded followed by a reperfusion. The results obtained show a similar response to the well-known occlusion test and reactive hyperemia could be visually observed, but future studies will include reference measurements, as they are essential to interpret the results with more confidence.

5. Conclusion

Given the limitations, our findings strengthen our hypothesis of a numeric 2 or 3-wavelength index with carefully selected wavelengths to accurately detect and monitor tissue ischemia. An index solely using reflectance information at 547 nm and 556 nm showed high diagnostic capability and compared well to the expected clinical time response. Compared to reference

Biomedical Optics EXPRESS

indices from literature, and tissue oxygenation estimates using an extended Beer-Lambert law, the proposed ischemia indices showed more robustness to varying experimental conditions and inter-subject variability. As proposed ischemia indices are computed fast, possibilities towards non-invasive and real-time monitoring of ischemic conditions of tissue are highlighted. As we traverse the path toward improved medical interventions, these findings hold substantial promise for enhancing patient care and clinical outcomes. Future research should delve into a broader range of subjects with diverse skin tones. Evaluating the sensitivity of the approach to different tissue types and real clinical scenarios, while including golden references of the ischemic state of the tissue is critical and is planned.

Disclosures. The authors declare no conflicts of interest.

Data availability. Data underlying the results presented in this paper are not publicly available at this time but may be obtained from the authors upon reasonable request.

Supplemental document. See Supplement 1 for supporting content.

References

1. J. A. Chin, E. C. Wang, and M. R. Kibbe, "Evaluation of hyperspectral technology for assessing the presence and severity of peripheral artery disease," J. Vasc. Surg. **54**(6), 1679–1688 (2011).
2. G. Lu and B. Fei, "Medical hyperspectral imaging: a review," J. Biomed. Opt. **19**(1), 010901 (2014).
3. G. Saiko, P. Lombardi, Y. Au, *et al.*, "Hyperspectral imaging in wound care: A systematic review," Int. Wound J. **17**(6), 1840–1856 (2020).
4. J. Shapey, Y. J. Xie, E. Nabavi, *et al.*, "Intraoperative multispectral and hyperspectral label-free imaging: A systematic review of in vivo clinical studies," J. Biophotonics **12**(9), e201800455 (2019).
5. M. Ewerlöf, M. Larsson, and E. G. Salerud, "Spatial and temporal skin blood volume and saturation estimation using a multispectral snapshot imaging camera," (SPIE, 2017), p. 1006814..
6. M. Ewerlof, T. Stromberg, M. Larsson, *et al.*, "Multispectral snapshot imaging of skin microcirculatory hemoglobin oxygen saturation using artificial neural networks trained on in vivo data," J. Biomed. Opt. **27**(3), 036004 (2022).
7. E. Zherebtsov, V. Dremin, A. Popov, *et al.*, "Hyperspectral imaging of human skin aided by artificial neural networks," Biomed. Opt. Express **10**(7), 3545 (2019).
8. K. K. Dreher, L. Ayala, M. Schellenberg, *et al.*, "Unsupervised domain transfer with conditional invertible neural networks," (2023).
9. J. R. Bauer, A. A. Bruins, J. Y. Hardeberg, *et al.*, "A spectral filter array camera for clinical monitoring and diagnosis: Proof of concept for skin oxygenation imaging," J. Imaging **5**(8), 66 (2019).
10. L. van Manen, W. Birkhoff, J. Eggermont, *et al.*, "Feasibility of a snapshot hyperspectral imaging for detection of local skin oxygenation," (SPIE-Intl Soc Optical Eng, 2019), p. 25.
11. L. van Manen, W. A. J. Birkhoff, J. Eggermont, *et al.*, "Detection of cutaneous oxygen saturation using a novel snapshot hyperspectral camera: a feasibility study," Quant. Imaging Med. Surg. **11**(9), 3966–3977 (2021).
12. H. Akbari, Y. Kosugi, K. Kojima, *et al.*, "Detection and analysis of the intestinal ischemia using visible and invisible hyperspectral imaging," IEEE Trans. Biomed. Eng. **57**(8), 2011–2017 (2010).
13. A. Holmer, J. Marotz, P. Wahl, *et al.*, "Hyperspectral imaging in perfusion and wound diagnostics - methods and algorithms for the determination of tissue parameters," Biomed. Eng. Tech. **63**(5), 547–556 (2018).
14. S. Hennig, B. Jansen-Winkeln, H. Köhler, *et al.*, "Novel intraoperative imaging of gastric tube perfusion during oncologic esophagectomy—a pilot study comparing hyperspectral imaging (hsi) and fluorescence imaging (fi) with indocyanine green (icg)," Cancers **14**(1), 97 (2021).
15. R. Sucher, T. Wagner, H. Koehler, *et al.*, "Hyperspectral imaging (hsi) of human kidney allografts," Ann. Surg. **276**(1), e48–e55 (2022).
16. S. J. Wirkert, "Multispectral image analysis in laparoscopy – a machine learning approach to live perfusion monitoring," (2018).
17. T. B. Fitzpatrick, "The validity and practicality of sun-reactive skin types i through vi," Arch. Dermatol. **124**(6), 869–871 (1988).
18. J. Pichette, T. Goossens, K. Vunckx, *et al.*, "Hyperspectral calibration method for CMOS-based hyperspectral sensors," (2017), p. 101100H.
19. R. Rosenberry and M. D. Nelson, "Reactive hyperemia: a review of methods, mechanisms, and considerations," Am. J. Physiol. Integr. Comp. Physiol. **318**(3), R605–R618 (2020).
20. L. Ayala, F. Isensee, S. J. Wirkert, *et al.*, "Band selection for oxygenation estimation with multispectral/hyperspectral imaging," Biomed. Opt. Express **13**(3), 1224–1242 (2022). Zn2prTimes Cited:0Cited References Count:46.
21. T. Chen, P. Yuen, M. Richardson, *et al.*, "Wavelength and model selection for hyperspectral imaging of tissue oxygen saturation," Imaging Sci. J. **63**(5), 290–295 (2015).
22. L. Finlayson, I. R. M. Barnard, L. McMillan, *et al.*, "Depth penetration of light into skin as a function of wavelength from 200 to 1000 nm," Photochem. Photobiol. **98**(4), 974–981 (2022).

Biomedical Optics EXPRESS

23. C. Ash, M. Dubec, K. Donne, *et al.*, "Effect of wavelength and beam width on penetration in light-tissue interaction using computational methods," Lasers Med. Sci. **32**(8), 1909–1918 (2017).
24. J. M. Gardner-Medwin, J. Taylor, I. Macdonald, *et al.*, "An investigation into variability in microvascular skin blood flow and the responses to transdermal delivery of acetylcholine at different sites in the forearm and hand," Br. J. Clin. Pharmacol. **43**(4), 391–397 (1997).
25. B. Abdelmalak, J. Cata, A. Bonilla, *et al.*, "Intraoperative tissue oxygenation and postoperative outcomes after major non-cardiac surgery: an observational study," Br. J. Anaesth. **110**(2), 241–249 (2013).